Acta Oncologica Vol. 33, No. 4, pp. 457–469, 1994

MICRODOSIMETRIC DESCRIPTION OF BEAM QUALITY AND BIOLOGICAL EFFECTIVENESS IN RADIATION THERAPY

ARIS TILIKIDIS and ANDERS BRAHME

Modern radiation therapy includes dosimetric and biological optimization methods aiming to improve the tumour control probability and reduce the unwanted reactions in healthy tissues. From this point of view the quality of the radiation beam is an important parameter that is not generally taken into account in clinical practice. The beam quality depends largely on the macroscopic absorption and scatter of the incident radiation but also on the microscopic fluctuations in the specific energy imparted within the cell nuclei in the patient. The radiation effect depends also on the complexity of the induced damage, the ability of the cells to control cell cycle progress and the efficiency and fidelity of the repair system. Therefore the conventional macrodosimetric quantities have to be complemented with microdosimetric quantities for an accurate description of the quality properties of the radiation beam. It is demonstrated that the DNA damage produced by sub keV electrons and high LET particles has a high probability to be lethal for the cell. These electrons may generate closely spaced double strand breaks or more general 'multiply damaged sites'. Such severely damaged sites may partly be due to the geometrical arrangement of double coiled DNA on the nucleosomes or triple coiled DNA in the cromatin fibre. This kind of damage has a large probability to be misrepaired when the DNA is opened up for repair and may therefore later result in cell death. Furthermore, it is shown that the reduced biological effect at ultra high LETs (>200 eV/nm) and at ultra short pulses of high dose rate low LET radiation most likely is due to increased radical-radical recombination in the 10 nm–10 ns domain. Based on microdosimetric measurements, significant quality variations in conventional therapeutic beams are detected particularly close to inhomogeneities, in the build-up region or in the presence of high LET contamination. These variations influence the biological effectiveness of the radiation beam and the steepness of the dose–effect relation, thus affecting in some cases the clinical radiotherapeutic outcome. It is shown that such effects may also explain the limited success of most trials with high LET radiations. A serious consideration of beam quality variations in treatment planning algorithms combined with dosimetric and radiobiological optimization of the treatment techniques may increase the probability of tumour control and minimize the unwanted acute and late reactions in healthy normal tissues.

The goal of modern radical radiation therapy is to deliver a curative dose distribution to the target tissues in order to eradicate all their clonogenic tumour cells while keeping the acute and late reactions in healthy normal tissues at a minimum. Advanced treatment planning algorithms allowing dose distributional and radiobiological response optimization are becoming available to individualize the treatment with respect to the shape of the target volume and the location of healthy organs at risk (1, 74). In this development of optimal dose delivery the influence of quality variations in the beam is often disregarded even if it may be used with advantage both to improve the local tumour control and to reduce adverse reactions in normal tissues.

For beams with a high linear energy transfer (LET), the depth variation of the radiation quality is of particular

Accepted 25 March 1994.
From the Department of Medical Radiation Physics, Karolinska Institutet and Stockholm University, Stockholm, Sweden.
Correspondence to: Dr Aris Tilikidis, Dept. of Medical Radiation Physics, Box 260, S-171 76 Stockholm, Sweden.

 ISSN 0284-186X

importance due to the high biological effectiveness around the Bragg peak and the reduced effect in the entrance or plateau region (2). If the Bragg peaks could be placed exclusively in the gross tumour region, high LET beams would be a definite clinical advantage. On the other hand, in beams where nuclear fragmentation products are present beyond the peak, the increasing dose and the associated biological effectiveness downstream of the tumour may cause clinical problems (3). Furthermore, the microdosimetric fluctuations and the associated non-uniform spatial distribution of the energy imparted in the tumour volume at the microscopic level may also be a clinical problem with high LET beams. This heterogeneity in the delivered dose reduces the steepness of the observed dose–effect relation and consequently the probability to achieve cure without causing severe damage to normal tissue (4). This phenomenon, together with the decreased capacity to repair high LET damage in normal tissues, which have to be irradiated when infiltrated by microscopic decease, may explain the limited success of high LET radiation therapy trials.

The advantage with low LET beams is on the contrary a more uniform microscopic energy deposition and a considerable potential for repair of radiation induced sublethal damage particularly in healthy normal tissues. For low LET beams the problem is instead a less optimal dose distribution combined with a risk of having a contamination by scattered radiation. This could be low energy electrons and photons, which may induce unwanted reactions in superficial normal tissues, or photonuclear reactions which may alter the biological effectiveness in deeply located tumour tissues.

The quality variations in the radiation field may decrease the dosimetric accuracy and thereby reduce the probability to control the tumour. This is particularly evident for tumours located in the build-up region, close to bone or metal interfaces and at the edges of the radiation field. The determination of the absorbed dose in these regions is affected by variations in the fluence and the stopping power but also by perturbations of the radiation field due to interface phenomena. Development of improved detectors, that minimize both fluence perturbation and energy dependence, may result in more accurate dosimetry (5). However, by such methods it will still be difficult to extract information concerning the quality radiation of the beam.

The random microscopic fluctuations of the energy depositions in subcellular biological targets cannot be accounted for using conventional dosimetric quantities which only describe the mean macroscopic dose level. Non-stochastic quantities such as the LET does not account for the finite range of low energy particles, the energy loss straggling along the track or the lateral extension of the secondary particle tracks in relation to the dimensions of the biological targets. This leads to significant differences between the mean energy loss and the real energy imparted to microscopic targets. Particularly for low energy electrons either in the form of track ends or secondary electrons but even more so in high LET beams with very dense δ-ray production along their tracks, the radiation induced damage can be considerable (Fig. 1 (6, 7)). For low and high LET alike, this implies that the majority of the critical biological damage is due to the low energy electrons that can cause locally severe damage to the nuclear DNA structure. This could be in the form of damage with higher complexity than double strand breaks, such as multiple local double strand breaks, or multiply damaged sites which seem to be quite difficult to repair by the cell.

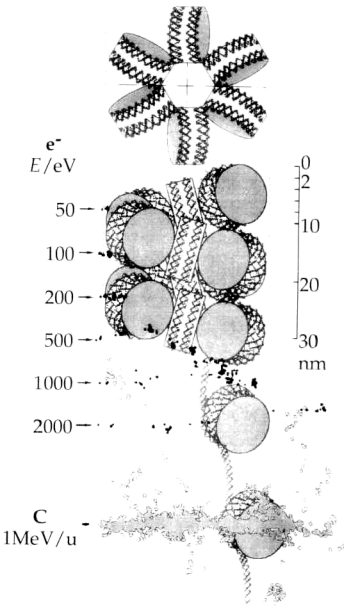

Fig. 1. Energy depositions by particle tracks in the chromatin fibre showing that the dominant critical radiation damage to DNA is produced by low energy electrons and δ-rays alone and not least when generated by a primary heavy charged particle.

The quality variations particularly in transition zones of therapeutic high energy electron and bremsstrahlung beams as well as in more conventional γ-ray beams can be obtained by applying microdosimetric techniques. This approach makes detailed measurements of the spatial distribution of energy depositions in relevant biological targets possible and allows a detailed quantitative analysis of the radiation field. A unique detector configuration with a wall-less proportional counter placed in a large vacuum chamber with a continuous flow of low density tissue equivalent gas, allows measurements at distances as short as a few μm from an interface (8–10). The wall-less detector minimizes the perturbation of the sampled radiation field at the same time as it can be used to get ordinary macrodosimetric information and microdosimetric spectra. The influence of the microdosimetric variance reduces the

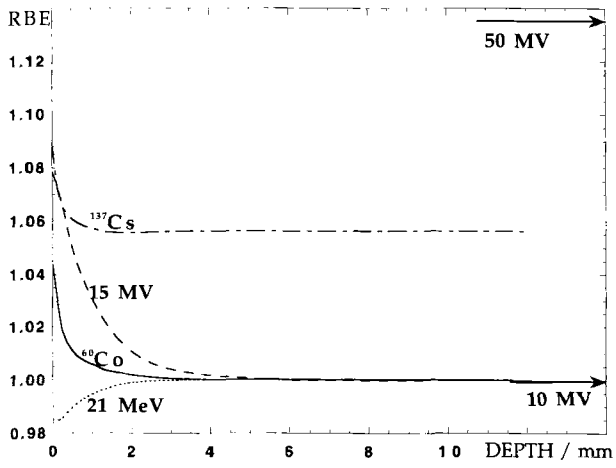

Fig. 2. Depth variation of the RBE in the build-up region of very clean, 20 cm^2 therapeutic photon and electron beams. The arrows indicate RBEs for 10 and 50 MV scanned beams measured at the therapeutic depth of 6 cm at 2 Gy doses. The data are determined using the methods of Tilikidis et al. (75).

steepness of the dose–effect gradient. Furthermore, in contamination-free bremsstrahlung and γ-ray beams, the dose–effect varies significantly with depth while only minor depth variations were observed in electron beams. The microdosimetric information may also be used to evaluate the depth dependence of the relative biological effectiveness (RBE) in therapeutic high energy electron and photon beams as well as in beams including contaminating neutrons of high biological effectiveness (75 (Fig. 2)). The increase in the biological effect at the surface is due to the pronounced faster build-up of electron and photon contamination and may be substantial for large clinical beams and short treatment distances (10).

The microdosimetric system described here allows even studies of the dosimetric properties of highly localized radionuclides. Particularly the properties of inhaled short range α-emitters with strongly non-uniform energy deposition at the subcellular level were studied. The large local doses imparted to the bronchial epithelium of the respiratory track in combination with the fast variations in radiation quality can cause serious health problems and have therefore been extensively studied (11). The results are of particular interest in connection with the risk of carcinogenesis associated with radon exposure. The same micro-dosimetric approach would also be ideal for determining biological and dosimetric information in targeted radiotherapy or diagnosis including areas where auger electron emitters (12) or boron capture therapy (13) with epithermal and high energy neutrons are used.

Physical and chemical aspects on radiation quality

During the physical interaction stage, charge particle tracks directly ionize the subcellular nuclear targets or water molecules that surround or bound directly to the DNA. Ionized or excited water molecules dissociate within 10^{-14} s into radical species whereas electrons from ionizations are rapidly thermalized and become trapped by surrounding water molecules. During the following chemical stage radicals diffuse away from the energy absorption centra and follow three possible reaction pathways, namely interactions with biologically important molecules causing indirect damage, recombination with each other resulting in H_2, H_2O and H_2O_2 molecules or they may become trapped by various radical scavengers. All the above reactions occur in a time scale shorter than 1 μs from the initial physical interaction and before the distribution of radicals reaches a final homogeneous state as a result of diffusion.

The indirect action in low LET beams is induced by free radicals which live some 5 to 10 ns and travel distances of the order of 10 nm. This type of action requires thus a close proximity between radicals and DNA molecules. Due to this proximity criterion it has been postulated that damage may even be induced by a combination of direct and indirect action close to the interface between the chromatin fibre and the surrounding water (14). For low LET radiation beams about 60% of the total lethal damage is particularly induced by OH and e^-_{aq} mainly acting on DNA sugar and bases; in high LET beams indirect action accounts for less than 20% of the total lethal damage induction (Fig. 3 (15, 16)). The reason for this difference can be found in the dense ionizations in the core of high LET tracks (cf. Fig. 4) and the associated high radical concentration. As is shown in Fig. 5, the lateral dimensions of the core are comparable with the diffusion and recombination distances involved in the motion of radicals. Consequently, in high LET beams, radical recombination within the dense ion core of the particle track reduces the biological effect from indirect radiation action in favour to direct action.

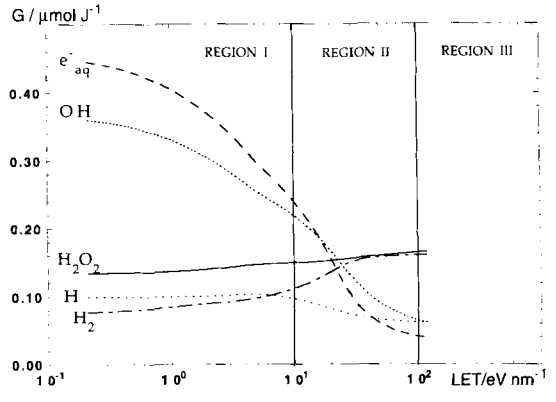

Fig. 3. LET dependence of the initial indirect acting decomposition products from water radiolysis and associated molecular recombination products. The regions indicated correspond to low, intermediate and high concentration of δ-rays around the track. In region II there is a competition between diffusion and recombination of radicals while in region III radical recombination dominates over diffusion. The figure is based on data from Magee & Chatterjee (71).

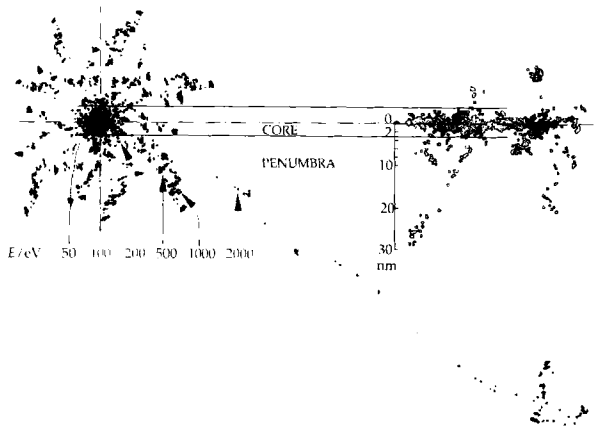

Fig. 4. The radial structure of the core (left panel) of a high LET carbon track (right panel) obtained by superposition of low energy electron tracks around the central core. The individual electron tracks are adopted from Paretzke (72).

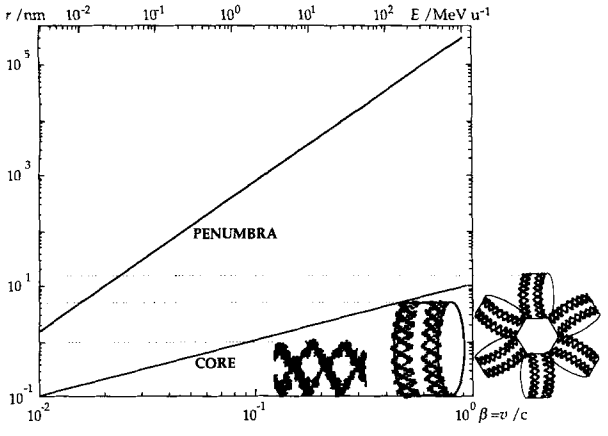

Fig. 5. The radial extension of the core and the penumbra region of high LET particles as function of the particles velocity expressed relative to the velocity of light. The core is defined as the region containing all the glancing collisional losses and those δ-rays completely stopped in this region. The horizontal lines in the figure indicate the size of the triple coiled DNA (chromatin fibre), 30 nm, double coiled DNA (chromatin), 11 nm, and the DNA double helix, 2 nm.

The primary biological damage is susceptible to modification particularly by reactions between reducing or oxidizing molecules and organic radicals. For low LET radiation the indirect mode of action is considerably affected by the presence or absence of oxygen. This is due to the preferential reaction of radicals with oxygen molecules rather than hydrogen donors from thiol containing protectors and the consequent fixation of the biological damage (17, 18). Thus, under hypoxic conditions, the induced lethal damage by OH radicals is reduced to about 20% of that under well oxygenated conditions. This is seen in the clinic as a reduced radiation sensitivity and reduced slope of the dose–effect relation particularly for tumours with high concentrations of hypoxic cells (19). In contrast, the radiation effects of high LET particles are only weakly dependent on the presence or absence of oxygen. Particularly at LETs in excess of 100 eV/nm, the oxygen effect disappears completely due to the reduced influence of oxygen related radical species on the biological effect.

Ultrahigh dose rates of ionizing radiation delivered within times shorter than the life time of the radical species, i.e. of the order of a few ns, result in a modified biological effectiveness as compared to conventional dose rates (20, 21). Particularly for normal clinical doses delivered in 30 ns pulses or less, the radiation sensitivity is reduced due to simultaneous presence of all radicals and consequent enhanced recombination. However, at higher doses (10ths of Gy) of low LET radiation an increased sensitivity may be observed due to increasing probability of closely spaced severely damaged targets similar to the situation along high LET tracks.

Critical damage due to the direct radiation action is most efficiently induced by electrons with energy below 1 keV in multinanometer size targets. For low LET radiation almost half the energy deposition is due to electrons with energies below a few keV (Fig. 6 and (22)). As is shown in Fig. 1 these low energy electrons have a high probability of inducing severe biological damage to triple coiled DNA. Furthermore, the similarities below about 1 keV in the slowing down spectrum explain the rather constant RBE for most low LET beams. For high LET particles a substantial part of the energy imparted is due to δ-rays from the track with energies below about 5 keV. The energy imparted by these electrons may be of the order of 80% or more of the total energy deposition by the track (23, 24). The similarities in the observed RBE values for low energy characteristic x-ray photons and α-particles (25) also indicate that δ-rays are the main cause of biological damage induced by high LET particles. The radial extension of the track depends primarily on the particle energy per nucleon and not on LET (cf. Fig. 5). By increasing the particle energy, more energy is transferred to δ-rays in the penumbra region which then rapidly increases in radii compared to the extension of the core. Thus, heavy ions with the same LET may have different biological effects depending on differences in the lateral extension and energy concentration in the penumbra.

The consequent differences in the microdosimetric distributions between low and high LET particles are shown in Fig. 6. These distributions are mainly formed by a combination of LET and chord length distributions in the target volume and the additional influence of the energy loss straggling across individual tracks. Low LET radiation results in rather broad distributions with mean energy depositions in the target up to about 30 eV/nm. The mean energy depositions by high LET particles are about 10 to 100 times higher than those for low LET. The microdosimetric distribution of a high LET particle can be described by the probability distribution of the combined action of multiple

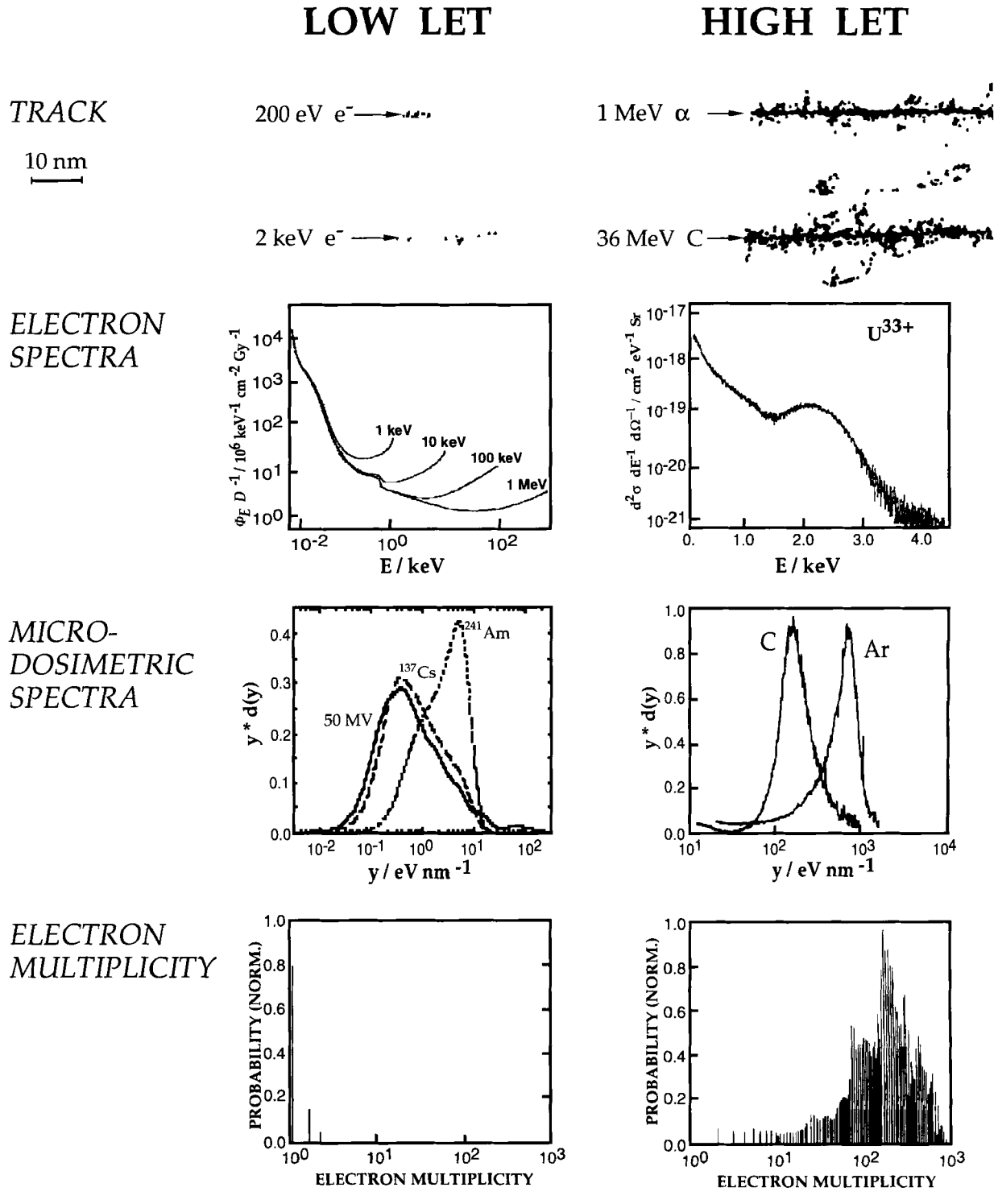

Fig. 6. Physical description of the energy deposition spectra in low and high LET beams. Track segments are adopted from Paretzke (72), the low LET slowing down spectra are from Hamm et al. (22), high LET generated δ-ray electron spectra from Schmidt-Böcking et al. (23), heavy ion microdosimetric distributions from Kliauga et al. (73), the low LET microdosimetric distributions are from Tilikidis et al. (8, 75) and the associated electron multiplicity distributions are from the present study.

low energy δ-rays events from a single track. The microdosimetric distribution of a ^{20}Ne ion beam (26) has been reconstructed in terms of the electron multiplicity distribution of low energy electrons (Fig. 6 bottom panels and Gustafsson, unpublished study) using an algorithm similar to that described by Lind (27) and Tilikidis et al. (75). It is thus seen that in μm sized volumes the energy depositions by high LET ions include a large number of electron

events rather than the single energy depositions commonly seen in low LET beams (cf. Fig. 6). In high LET beams it is rather difficult to achieve homogeneous irradiation conditions of all the clonogenic tumour cells due to the high energy deposition along the track of the incident particles. At low doses the mean specific energy approaches a constant value corresponding to the energy deposition by a single track whereas the number of affected targets is influenced by the frequency of zero events, i.e. particles passing but not interacting with the target volume. With increasing dose the mean specific energy and the absorbed dose approach each other while the number of affected targets is constant since all of them are hit. Particularly for heavy ions substantially higher doses than those applied in radiotherapy are required to obtain a homogeneous microscopic dose delivery on the subcellular scale comparable to low LET radiations.

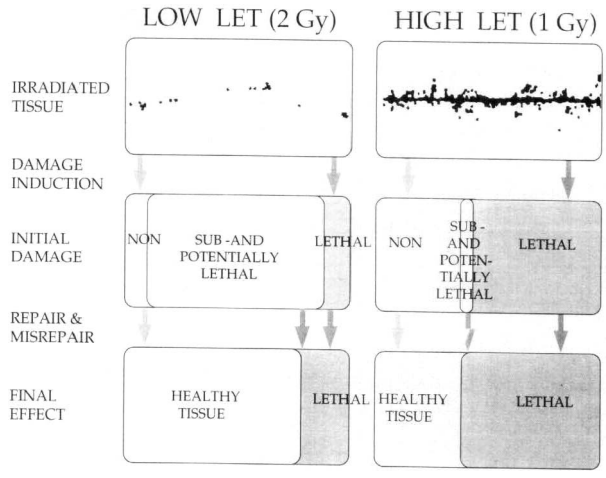

Fig. 7. Schematic presentation of the influence of radiation quality on the type, relative frequency and effectiveness of the radiation induced damage and the associated capacity of the repair mechanism. For high and low LET the α and β values are 0.08 and 0.026, and 0.835 and 0.001 respectively.

Biological aspects on radiation quality

The damage to nuclear DNA by direct and indirect action of ionizing radiation may be expressed in terms of double strand breaks (DSB), single strand breaks (SSB), sugar or base damage, DNA-DNA crosslinks, DNA-protein crosslinks and complex combination of the same. A significant part of the induced damage is sublethal or potentially lethal depending on the postirradiation conditions. Sublethal damage may be repaired by enzymatic and other mechanisms, such as excision repair if sufficient time is allowed before the evaluation of the biological endpoint. Lack of repair can be attributed to factors like complexity of damage, rejoining fidelity, repair inhibition and available time. Other factors influencing the repair capacity are capability of the cell to block cell cycle progress until all potentially lethal lesions have been repaired and the degree of condensation of the DNA and the stage in the cell cycle. For a particular biological system and endpoint damage repair is also affected by the LET of the radiation beam, the oxygenation of the cells and even the dose rate (cf. Figs. 7 and 8).

For mammalian cells the quasi exponential repair function is fast for low LET radiation indicating that a large part of the induced sublethal damage is repaired within a few hours. For the synergistic effects observed in mammalian cells irradiated with combined high and low LET beams it has been shown that some sublethal damage exists even after irradiation with high LET ions (28, 29). However, in high LET beams the amount of repairable damage is substantially reduced, as seen by the decreased shoulder and the pure exponential shape of the survival curve at LET values of 150–200 eV/nm (30, 31), disappears completely at LETs above about 10^3 eV/nm (32). Furthermore, the steepness of the time-dependent repair function is substantially reduced and the time needed for repair is 2 to 5 times longer than for low LET beams (33–35). This indicates that the biological damage induced by high LET beams is more complex than that induced by low LET radiation.

The enormous capability of cells to repair simpler forms of DNA damage results in only about 1% unrejoined DNA breaks per cell and Gy of low LET radiation. Lethality as a biological endpoint is likely to be associated with multiple closely spaced DSBs which may be very complex to repair with a high degree of fidelity due to increased risk of misrepair and loss of DNA. Thus, only about 4% of the unrejoined DNA breaks mentioned above, i.e. 0.04% of the initial DNA damage, will lead to lethality. The formation of critical lesions requires close proximity between severe energy depositions or dense clusters of sublethal or radical damage The differences in RBE obtained by different high LET particles with the same LET (36) indicate, however, that closely induced DSBs may be the most severe form of lethal damage even more so than highly complex damage.

The biological effect of a radiation beam may be macroscopically described by its RBE. For a particular biological endpoint and radiation quality the RBE is affected by the fractionation scheme and the dose rate applied. The biological effectiveness is furthermore strongly dependent on the stage in the cell cycle. In low LET beams it is well documented that cells are particularly sensitive during the mitotic and G2 phase and resistant during the late S-phase. With increasing LET the variations in the age response during the cell cycle decrease and disappear completely for heavy ions in the LET range above 300 eV/nm ((37, 38) and third panel Fig. 8). The RBE-LET function also reaches a maximum at LET values between 100 and 300 eV/nm. To be more accurate, the RBE curves show discrete maxima which are characteristic for each particu-

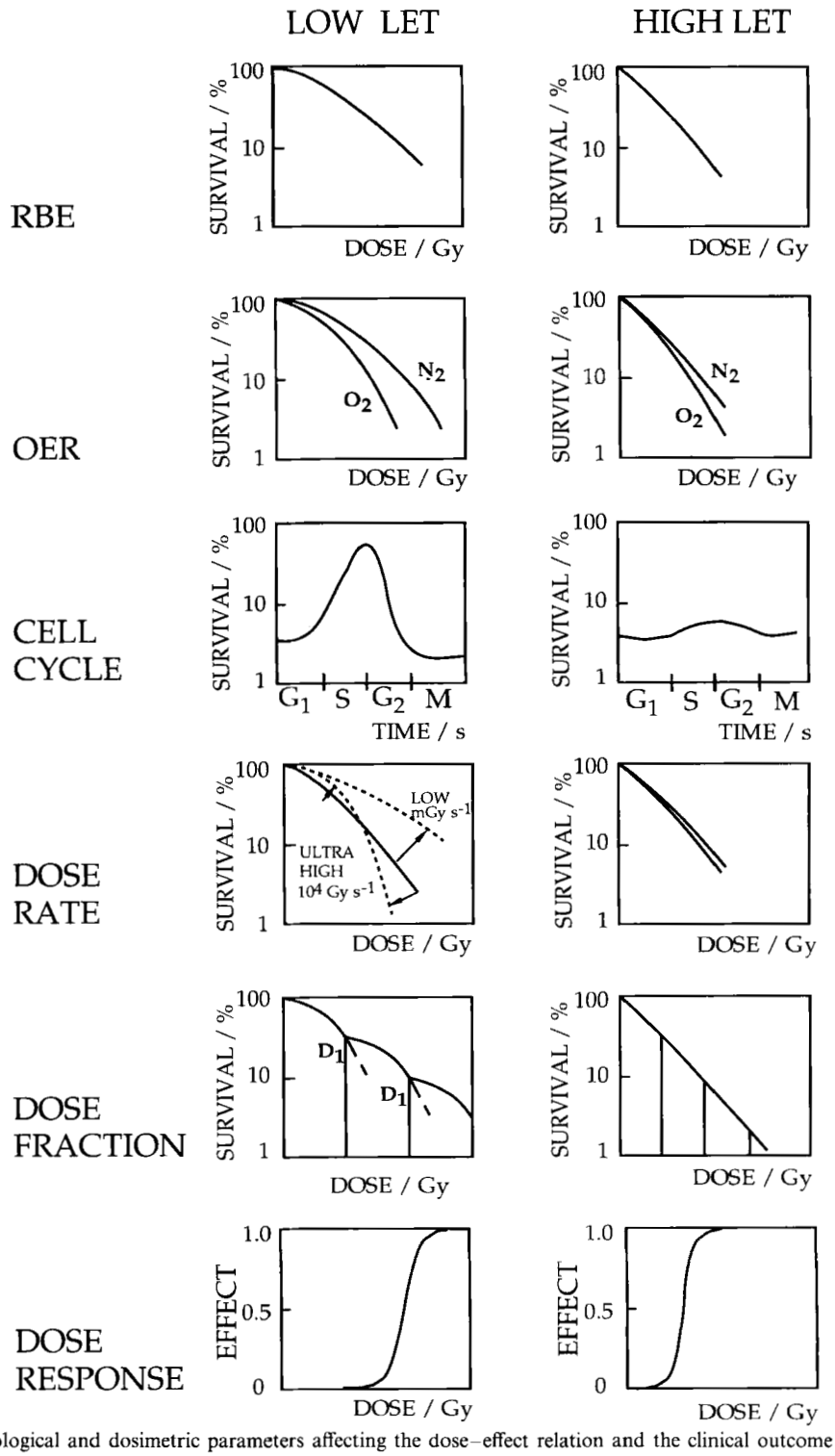

Fig. 8. The main biological and dosimetric parameters affecting the dose–effect relation and the clinical outcome in radiation therapy.

lar ion type and biological endpoint (39). Above the peak the RBE decreases rapidly as seen in Fig. 9. This is due both to the decreasing interaction cross-section as a result of a shrinking core radius and to the associated increase in the recombination probability of radicals and charges due to the extreme proximity and simultaneous presence of the species (16, 39, 75).

The biological response of a mammalian cell population to a given irradiation can be conveniently quantified by the so-called linear-quadratic (LQ) model (40). In terms of this

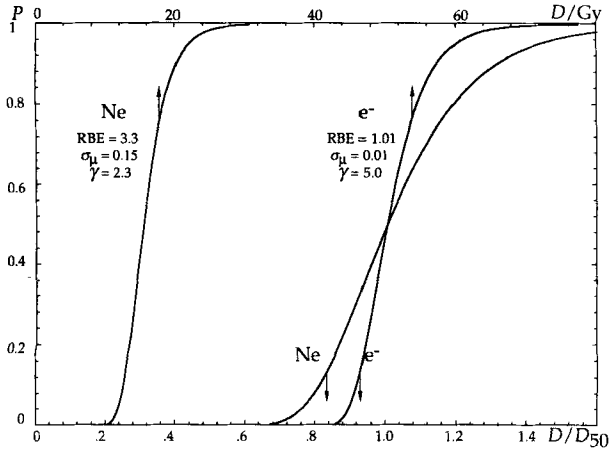

Fig. 9. Influence of the microdosimetric relative variance on the steepness of the dose–effect relationship. The large variance associated with high LET beams decreases the dose–effect gradient substantially.

model the probability, P, of controlling a tumour with N initial clonogenic cells by a total dose, D, given in n well-separated fractions, is given by

$$P(D) = e^{-Ne^{-\alpha D-\beta D^2/n}} = e^{-e^{\gamma e-\alpha D-\beta D^2/n}} \quad [1]$$

The term α may be interpreted as a measure of the probability of induced irreparable injury as expressed by the linear component of the survival curve whereas the β term is related to the cumulation of repairable damage leading to the curved part of the survival curve. The term γ is the normalized dose–response gradient of the dose–effect relation which, for a constant dose per fraction, is proportional to the logarithm of the clonogen number given by $\gamma = \ln N/e$ (Fig. 8, (19)).

Curative radiation therapy of malignancies is helped by the fact that tumours with high radioresponsiveness have a small repair potential and thus show a high α/β ratio in contrast to late reacting tissues (41, 42). However, the tissue specific α/β ratio depends not only on the properties of the particular tissues but also on the radiation quality and dosimetric characteristics of the beam and consequently on the fluctuations of the microscopic energy depositions in the individual cells of the irradiated tissues. These factors may also affect the RBE at different depths in low LET therapeutic beams. By approximating Eq. [1] above by an integral over a normal distribution, the associated apparent relative standard deviation, σ_C, of the dose required for clinical tumour eradication becomes

$$\sigma_C = \frac{1}{\sqrt{2\pi}\gamma_C}\left\{1 + \frac{1}{4\pi\gamma_C^2} + \frac{1}{32\pi^2\gamma_C^4} + \cdots\right\} \quad [2]$$

where γ_C is the normalized gradient of the clinically observed dose–effect relation (19, 43). This apparent uncertainty in the clinical control of the tumour is due to a number of biological and energy deposition factors. The biological part, σ_B, is a mean value over the generally large number of patients that have been treated; it will also depend on factors, such as the apparent variance in the threshold dose which depends on the toal number of clonogenic cells, intra- and intertumour variability due to factors like mutation status, heterogeneous oxygenation, fractionation effects, etc. (44). The dosimetric and microdosimetric factors will be discussed in more detail in the next section.

Microdosimetric aspects on radiation quality

The outcome of radiation therapy regarding the eradication of all clonogenic tumour cells depends on the biological variability of the tumour cell sensitivity, the local deviations from homogeneous macroscopic dose delivery over the target volume, and the microscopic fluctuations of the specific energy imparted to the cell nuclei of the clonogenic cells. The stochastic nature of energy depositions is expressed by the specific energy, z, that is the energy imparted to a finite volume per unit mass

$$z = \frac{d\varepsilon}{dm} \quad [3]$$

The stochastic variation of z around its local mean value, $\bar{z}(\vec{r})$, identical to the local macroscopic absorbed dose, $D(\vec{r})$, increases with decreasing dose and increasing LET. The statistical distribution function of z, $f(z, D(\vec{r}))\,dz$, represents the probability of depositing a specific energy between z and $z + dz$. This function can be expressed by an appropriate sum over all possible event multiplicities and their associated contributions accurately given by the Poisson distribution (48)

$$f(z, D(\vec{r})) = \sum_{\nu=0}^{\infty} \frac{e^{-\bar{\nu}}\bar{n}^{\nu}}{\nu!} f_\nu(z) \quad [4]$$

where $f_\nu(z)$ is the probability distribution for exactly ν events given by the ν-fold convolution of the distribution for one event. Furthermore, $f_1(z)$, $\bar{\nu} = \bar{z}(\vec{r})/\bar{z}_1$ is the mean event number and $\bar{z}_1$ is the mean specific energy deposited by a single event.

The mean specific energy at a point $\vec{r}$ is related to the local absorbed dose through the relation

$$D(\vec{r}) = \lim_{d^3r \to 0} \bar{z}(\vec{r}) \quad [5]$$

The spatial mean value of the classical macroscopic dose distribution in a tumour or organ of density $\rho(\vec{r})$ at the position $\vec{r}$ is given by

$$\bar{D} = \frac{\iiint D(\vec{r})\rho(\vec{r})\,d^3r}{\iiint \rho(\vec{r})\,d^3r} \quad [6]$$

and its relative variance

$$\sigma_D^2 = \frac{\iiint (D(\vec{r}) - \bar{D})^2\rho(\vec{r})\,d^3r}{\left(\iiint D(\vec{r})\rho(\vec{r})\,d^3r\right)^2} \quad [7]$$

These first two moments of the dose distribution are of considerable clinical value since together they determine the first two terms of the probability to eradicate a tumour or damage a normal tissue volume by a dose distribution $D(\vec{r})$ (45). However, in clinical practice, the microdosimetric heterogeneity of the dose distribution is also highly relevant (46) and strictly speaking σ_D^2 should be replaced by σ_z^2, i.e. the relative variance of the specific energy at subcellular level for the organ in question (5). In this general case the tumour control probability takes the form

$$P(D(\vec{r})) = P(\bar{D}) - \frac{\gamma^2}{2P(\bar{D})}\sigma_z^2 \qquad [8]$$

For an irradiated tissue volume σ_z^2 is affected both by the local variations of the macroscopic dose at each point $\vec{r}$ over the irradiated volume and the local microdosimetric fluctuations of the energy imparted in all clonogenic tumour cells The relative variance of the specific energy in a tissue volume is by definition given by

$$\begin{aligned}\sigma_z^2 &= \frac{\iiiint (z-\bar{D})^2 f(z, D(\vec{r}))\, \mathrm{d}z\, \rho(\vec{r})\, \mathrm{d}^3r}{\left(\iiiint z f(z, D(\vec{r}))\, \mathrm{d}z\, \rho(\vec{r})\, \mathrm{d}^3r\right)^2} \\ &= \frac{\iiiint ((z-\bar{z}(\vec{r})) + (D(\vec{r})-\bar{D}))^2 f(z, D(\vec{r}))\, \mathrm{d}z\, \rho(\vec{r})\, \mathrm{d}^3r}{\bar{D}^2} \\ &= \frac{\iiiint ((z-\bar{z}(\vec{r}))^2 + (D(\vec{r})-\bar{D}))^2 + 2(z-\bar{z}(\vec{r}))(D(\vec{r})-\bar{D}))f(z, D(\vec{r}))\, \mathrm{d}z\, \rho(\vec{r})\, \mathrm{d}^3r}{\bar{D}^2}\end{aligned} \qquad [9]$$

The integral over the first quadratic term of Eq. [9] represents the mean microdosimetric variance over the target volume of interest, $\overline{\sigma_\mu^2}$, since after integration over z we obtain

$$\frac{\iiiint ((z-\bar{z}(\vec{r}))^2 f(z, D(\vec{r}))\, \mathrm{d}z\, \rho(\vec{r})\, \mathrm{d}^3r}{\bar{D}^2} = \iiint \sigma_\mu^2(\vec{r})\rho(\vec{r})\, \mathrm{d}^3r = \overline{\sigma_\mu^2} \qquad [10]$$

The integral over the second quadratic term in Eq. [9] represents the relative variance of the macrodosimetric dose distribution, σ_m^2, according to Eq. [7]

$$\frac{\iiiint (D(\vec{r})-\bar{D})^2 f(z, D(\vec{r}))\, \mathrm{d}z\, \rho(\vec{r})\, \mathrm{d}^3r}{\bar{D}^2} = \frac{\iiint (D(\vec{r})-\bar{D})^2 \rho(\vec{r})\, \mathrm{d}^3r}{\bar{D}^2} = \sigma_m^2 \qquad [11]$$

The last double product term represents the covariance, $C_{z,D(\vec{r})}$, between z and $D(\vec{r})$. This term becomes

$$\begin{aligned}C_{z,D(\vec{r})} &= \iiiint (z-\bar{z}(\vec{r}))(D(\vec{r})-\bar{D}) f(z, D(\vec{r}))\, \mathrm{d}z\, \rho(\vec{r})\, \mathrm{d}^3r \\ &= \iiiint (zD(\vec{r}) - z\bar{D} - \bar{z}(\vec{r})D(\vec{r}) + \bar{z}(\vec{r})\bar{D}) f(z, D(\vec{r}))\, \mathrm{d}z\, \rho(\vec{r})\, \mathrm{d}^3r \\ &= \iiiint (\bar{z}(\vec{r})D(\vec{r}) - \bar{z}(\vec{r})\bar{D} - \bar{z}(\vec{r})D(\vec{r}) + \bar{z}(\vec{r})\bar{D})\rho(\vec{r})\, \mathrm{d}^3r \equiv 0\end{aligned} \qquad [12]$$

and is identical to zero since the mean value of one of the variables, $\bar{z}(\vec{r})$, is equal to the other independent variable, $D(\vec{r})$. The relative variance in the specific energy over the whole irradiated tissue volume is thus equal to the sum of the mean microdosimetric, $\overline{\sigma_\mu^2}$, and the macrodosimetric, σ_m^2, relative variances according to

$$\sigma_z^2 = \overline{\sigma_\mu^2} + \sigma_m^2 \qquad [13]$$

The total relative variance in the clinical response of an irradiated cell population, σ_C^2, may be approximated by the sum of the intrinsic biological variance, σ_B^2, and the variance in the energy imparted, σ_z^2, (4)

$$\sigma_C^2 = \sigma_B^2 + \sigma_z^2 \qquad [14]$$

This relation allows the determination of the clinically observable normalized gradient of the dose–response relation, γ_C, through Eq. [2] above provided σ_B^2 is known as is discussed in the section 'Biological aspects on radiation quality'.

The microscopic variance of a multievent distribution, $f(z, D(\vec{r}))$, is directly related to the quality of the radiation beam. For a particular beam consisting of the distributions $f(z_1), f(z_2), \ldots, f(z_j)$ of j different radiation qualities, each with relative dose constributions $\bar{D}_j/\bar{D}$, the mean microscopic relative variance in z, $\overline{\sigma_\mu^2}$, becomes

$$\overline{\sigma_\mu^2} = \frac{1}{\bar{D}} \sum_{k=1}^{j} \bar{D}_j \frac{\overline{z_{1_k}^2}}{z_{1_k}} \qquad [15]$$

The build-up region of a therapeutic beam is a concrete example where a large change in radiation quality and thus in microdosimetric variance is combined with rapid changes in the mean absorbed dose and therefore in the macrodosimetric variance. Dependent on the particular beam properties and the amount of contaminating components, the above variances may decrease the slope of the dose–effect relation (cf. Eq. 2, (11, 12), and Fig. 9). This may influence the accurate determination of the α/β ratio for acute and late reactions like erythema, desquamation, telangiectasia and subcutaneous fibrosis observed in shallow located tissues (47, 48).

The microdosimetric spectrum of a particular radiation modality may even give appropriate information on

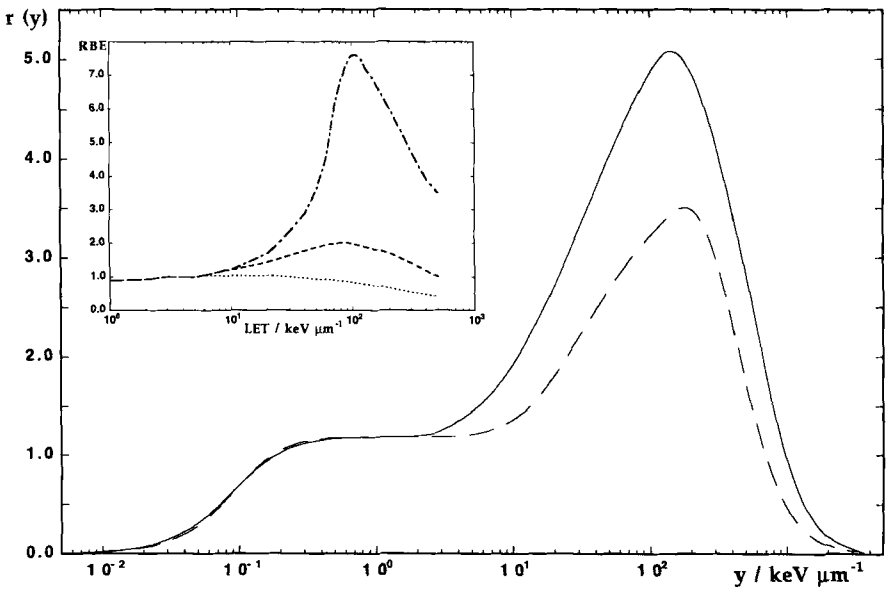

Fig. 10. The biological response functions for high ($\approx$0.6) and low ($\approx$0.02) survival levels (full and long broken curves respectively) calculated using single event microdosimetric distributions and experimental RBE values for a number of low and high LET radiation qualities (75). In the insert, RBE values for single track lethal damage (chain curve), DNA double strand breaks (short broken curve) and DNA single strand breaks (dotted curve), redrawn from Barendsen (35) are shown for comparison.

the biological effectiveness. This procedure requires the determination of a relative biological effect function, $r(y)$, from a number of radiation modalities with known microdosimetric characterization and established biological effectiveness for a certain biological endpoint. The biological effectiveness, R_m, of the particular radiation modality for the specific biological endpoint may then be expressed as the integral value of its normalized dose weighted microdosimetric single event distribution, $d_m(y)$, weighted by the relative biological effect function according to the equation

$$R_m = \int_0^\infty r(y)\, d_m(y)\, dy \qquad [16]$$

Applications of this approach in the accurate estimation of the relative biological effectiveness of radiotherapeutic high energy beams are given by Pihet et al. (49) and Tilikidis et al. (75) (cf. Fig. 10).

Dosimetric aspects on radiation quality

The dosimetric properties and quality characteristics of high energy therapeutic beams are strongly affected by the beam generating devices such as the target and the beam flattening system. Other devices affecting the beam quality are transmission monitors, collimators and other components placed in the treatment head between the source and the patient, such as the air volume, beam blocks, etc. Bremsstrahlung beams are affected by contaminating electrons, photons and even neutrons produced by photonuclear reactions in the target and filters placed in the treatment head. Electron beams are influenced by the initial angular and energy spread of the intrinsic accelerator beam and that from scattering foils, transmission monitors, etc., but also by secondary electrons and bremsstrahlung photons. For conventional high energy bremsstrahlung beams the main source of contaminating electrons is the beam flattening filter whereas in low energy beams electrons generated in the air by photons give a substantial contribution to the dose in superficial tissues. The contamination from electrons generated in the beam flattening filter and wedges is minimized using medium atomic number materials for which an optimal ratio between a high probability for multiple scattering and relatively low probability for photon interactions is obtained (50). The collimator generated electron contamination can be reduced using high density materials at all collimator edges directly hit by the beam. In modern treatment units with scanned beams, as the racetrack microtron, helium gas is used within the treatment head, thus reducing photon-generated contaminating electrons from the gas volume by a factor of almost 10. Electrons and positrons from pair production events in the target can, due to the absence of flattening filter in these units, reach the treatment volume. For this reason a purging magnet situated immediately downstream of the target can be used to sweep the charged particle contamination out of the useful beam (50–52).

In addition to the electron contamination, low energy photons generated during the production of the bremsstrahlung beam or in scattering interactions with the collimators of the treatment unit, may also contaminate the

beam especially in low energy machines. The scattered photon contribution to the absorbed dose in bremsstrahlung beams is about 3–5% of the total dose (53, 54). Their influence will increase the dose and the stopping power ratio in the build-up region of the radiation beam. However, the combined effect of a photon and electron contamination may reduce this variation (55). In gamma ray beams the contribution from source scattered low-energy photons is often significant. Depending on the size and type of the encapsulation of the gamma source, the dose contribution from scattered photons may be up to 20% of the primary photon dose (56, 57). All contamination affects the build-up region of the photon depth dose curve thus decreasing the depth of dose maximum. This is particularly important at large field sizes where the electron contamination increases substantially due to lower effect of scatter filtering in the air. Furthermore, contamination affects both the penumbra and beam uniformity thus altering the therapeutic beam properties.

Photonuclear reactions in tissues irradiated with bremsstrahlung beams result in the production of high LET particles with minor contribution to the absorbed dose but with significant biological effectiveness (58–60).

The build-up region of an electron beam is characterized by a superficial very rapid increase of the slowing-down spectrum of low energy secondary electrons with wide angular distributions and an extended build-up region caused by the multiple scattering of the primary electrons (61, 62). Scattered electrons decrease the depth of dose maximum and increase the relative dose in the build-up region which is a disadvantage especially at high energies (63). The maximum fluence and consequently the maximum absorbed dose in electron beams occurs when a balance is achieved in the angular distribution of primary electrons between increasing multiple scatter and increasing loss due to wide scattering angles and range straggling.

Rapid changes of the beam quality and the absorbed dose in bremsstrahlung beams are also observed close to the interfaces between tissue and bone, lung or metal objects located in the irradiated volume and even at the edges of the radiation field and at material interfaces in general (cf. Fig. 11). These rapid quality variations are mainly a result of the local transport of secondary electrons including multiple scattering, energy loss straggling and δ-ray productions and, for high atomic number interfaces, annihilation, photon scatter and attenuation (50, 64). Similar variations are also observed in electron beams due to pronounced electron scatter effects which affect the absorbed dose both in the direction of the beam and laterally (65, 66). Many of these beam properties cannot be studied in the transition regions mentioned above using conventional dosimetric techniques, such as ion chambers due to the perturbation of the electron fluence associated with scattering phenomena in the detector as well as perturbation of the photon fluence by the chamber wall.

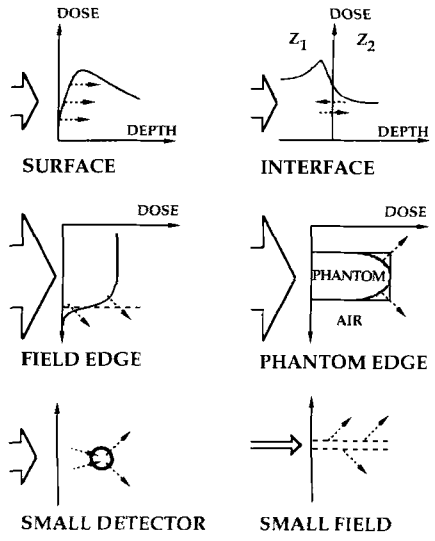

Fig. 11. Illustration of situations where the equilibrium in the transport of secondary charged particles (dashed arrows) is perturbed.

Even specifically designed plane parallel ionization chambers are affected by such perturbations thus overestimating the surface dose (67, 68). Particularly in the build-up region the non-equilibrium conditions and the presence of low energy contaminating components alter the relative contribution to the dose from starters, stoppers and insiders, thus affecting the application of conventional cavity theories (69, 70). In all these cases the wall-less microdosimetric technique is the ideal tool for simultaneous dosimetry and beam quality determination.

Conclusions

Microdosimetric techniques allow accurate determination of the radiation quality and its variations in therapeutic beams. Large fluctuations in the microdosimetric energy depositions in the tumour cells result in a strongly heterogeneous dose distribution and therefore a reduced steepness of the dose–effect relation and an altered and often reduced probability to achieve a curative treatment. This is evident particularly for high LET beams where the relative variance in the microscopic energy depositions is increased also due to the lower dose required to induce a given biological effect. Even fairly conventional low LET therapeutic beams with high degrees of photon, electron or neutron contamination are affected but to a lesser extent.

It is also shown that the DNA damage produced by sub keV electrons and high LET particles has a high probability to be lethal for the cell. These electrons may generate closely spaced double strand breaks or more general 'multiply damaged sites'. Such severely damaged sites may partly be due to the geometrical arrangement of double coiled DNA on the nucleosomes or triple coiled DNA in the chromatin fibre. This kind of damage has a large

probability to be misrepaired when the DNA is opened up for repair and may therefore later result in cell death. Furthermore, it is demonstrated that the reduced biological effect at ultra-high LETs (>200 eV/nm) and at ultra-short pulses of high dose rate low LET radiation most likely is due to increased radical-radical recombination in the 10 nm–10 ns domain. The microdosimetric distribution of the energy deposition by a particular radiation beam can be used together with known RBE data for a particular biological endpoint to accurately predict the RBE of the beam for that endpoint at a certain therapeutic dose level. This approach thus allows the use of physical methods to determine the biological response during radiation therapy by appropriate calibration against known biological data.

Finally, the improved integration of radiation quality parameters in the physical and biological optimization of radiation therapy is expected to allow increased tumour doses and decreased normal tissue damage and thereby further improve the clinical outcome.

REFERENCES

1. Lind BK, Brahme A. Optimization of radiation therapy dose distributions using scanned electron and photon beams and multileaf collimators. Proc. 9th Int. Conf. on Computers in Radiation Therapy. Elsevier, 1987: 235–9.
2. Blakely EA, Tobias CA, Yang TCH, Smith KC, Lyman JT. Inactivation of human kidney cells by high-energy monoenergetic heavy-ion beams. Radiat Res 1979; 80: 122–60.
3. Ito A, Henkelman RM. Microdosimetry of the pion beam at TRIUMF. Radiat Res 1980; 82: 413–29.
4. Lindborg L, Brahme A. Influence of microdosimetric quantities on observed dose-response relationships in radiation therapy. Radiat Res 1990; 124: 23–8.
5. Nilsson B, Montelius A, Andreo P. A study of interface effects in ^{60}Co beams using a thin-walled parallel plate ionization chamber. Med Phys 1992; 19: 1413–21.
6. Kellerer AM, Chmelevsky D. Criteria for the applicability of LET. Radiat Res 1975; 63: 226–34.
7. Goodhead DT, Nikjoo H. Track structure analysis of ultrasoft X-rays compared to high- and low-LET radiations. Int J Radiat Biol 1989; 55: 513–29.
8. Tilikidis A, Brahme A, Lindborg L. Microdosimetry in the build-up region of gamma ray beams. Radiat Prot Dos 1990; 31: 227–33.
9. Tilikidis A, Iacobaeus C, Brahme A. Microdosimetric measurements in the build-up region of very pure high-energy photon and electron beams. Phys Med Biol 1993; 38: 765–84.
10. Tilikidis A. Skog S, Brahme A. Influence of radiation quality changes on microdosimetric variance and dose-response relations. Radiat Prot Dos 1994; 52: 43–9.
11. Grinborg JE, Lindborg L, Tilikidis A, Falk R. Dosimetry around hot particles with microdosimetric techniques. Radiat Prot Dos 1990; 31: 389–94.
12. Makrigiorgos G, Adelstein SJ, Kasis AI. Auger electron emitters: Insights gained from in vitro experiments. Radiat Environ Biophys 1990; 29: 75–91.
13. Pettersson O-A. Boron neutron capture therapy. Binding of boron compounds to cultured cells and studies on therapeutic effects. (Dissertation) Uppsala University, 1992.
14. Frankenberg D, Frankenberg-Schwager M, Harbich R. The contribution of OH* in densely ionising electron track ends or particle tracks to the induction of DNA double strand breaks. Radiat Prot Dos 1990; 31: 249–52.
15. Roots R, Chatterjee A, Chang P. Lammel L, Blakely E. Characterization of hydroxyl radical-induced damage after sparesely and densely ionizing radiation. Int J Radiat Biol 1985; 47: 157–66.
16. Holley WR, Chatterjee A, Magee JL. Production of DNA strand breaks by direct effects of hevy charged particles. Radiat Res 1991; 121: 161–8.
17. Holian J, Garisson WM. Reconstitution mechanisms in the radiolysis of aqueous biochemical systems: Inhibitive effects of thiols. Nature 1969; 221: 57.
18. Prise KM, Davies S, Michael BN. A comparison of the chemical repair rates of free radical precursors of DNA damage and cell killing in Chinese hamster V79 cells. Int J Radiat Biol 1992; 61: 721–8.
19. Källman P, Ågren A, Brahme A. Tumour and normal tissue responses to fractionated non-uniform dose delivery. Int J Radiat Biol 1992; 62: 249–62.
20. Todd P, Winchell SH, Feola JM, Jones GE. Pulsed high-intensity roentgen rays. Acta Radiol Ther Phys Biol 1968; 7: 22–6.
21. Svensson H, Brahme A. Fundamentals of electron beam dosimetry. In: Florence CH, Chu FCH, Laughlin JS, eds. Proceedings of the symposium on electron beam therapy. New York: Memorial Sloan-Kettering Cancer Center, 1981: 17–30.
22. Hamm RN, Wright HA, Katz R, Turner JE, Ritchie RH. Calculated yields and slowing-down spectra for electrons in liquid water: Implications for electron and photon RBE. Phys. Med Biol 1978; 23: 1149–61.
23. Schmidt-Böcking H, Ramm U, Kraft G, et al. δ-electron emission in fast heavy ion atom collisions. Adv Space Res 1992; 12: 7–15.
24. Kraft G, Krämer, Scholz M. LET, track structure and models. Radiat Environ Biophys 1992; 31: 161–80.
25. Frankenberg D, Frankenberg-Schwager M, Blöcher D, Harbich R. Evidence for DNA double-strand breaks as the critical lesion in yeast cells irradiated with sparsely or densely ionising radiation under oxic or anoxic conditions. Radiat Res 1981; 88: 524–32.
26. Gross W, Dicello J, Colvett RD. The dosimetry and microdosimetry of 5.7 GeV neon ions. In: Annual report on research project, Radiological Research Laboratory, Columbia University NY, 1974: 88–115 COO 3243-3, United States Atomic Energy Commission.
27. Lind BK. Properties of an algorithm for solving the inverse problem in radiation therapy. Inverse Problems 1990; 6: 415–26.
28. Ngo FQH, Blakely E, Tobias C. Sequential exposures of mammalian cells to low- and high LET radiations. Radiat Res 1981; 87: 59–78.
29. Suzuki S. Survival of Chinese hamster V79 cells after irradiation with a mixture of neutrons and ^{60}Co γ rays: experimental and theoretical analysis of mixed irradiation. Radiat Res 1993; 133: 327–33.
30. Barendsen GW. Response of cultured cells, tumors and normal tissues to radiations of different linear energy transfer. Curr Top Radiat Res 1968; 4: 295–356.
31. Todd PW. Heavy ion irradiation of human and Chinese hamster cells in vitro. Radiat Res 1975; 61: 288–97.
32. Heilmann J, Rink H, Taucher-Scholz G, Kraft G. DNA strand break induction and rejoining and cellular recovery in mammalian cells after heavy-ion irradiation. Radiat Res 1993; 135: 46–55.

33. Ward JF. DNA damage produced by ionizing radiation in mammalian cells: identities, mechanisms and repairability. Prog Nucleic Acid Res Mol Biol 1988; 35: 95–125.
34. Ward JF. The yield of DNA double-strand breaks produced intracellularly by ionizing radiation: a review. Int J Radiat Biol 1990; 57: 1141–50.
35. Barendsen GW. Mechanisms of cell reproductive death and shapes of radiation dose-survival curves of mammalian cells. Int J Radiat Biol 1990; 57: 885–96.
36. Goodhead DT, Belli M, Mill AJ, et al. Direct comparison between protons and alpha-particles of the same LET: I. Irradiation methods and inactivation of asynchronous V79, HeLa and C3H10T1/2 cells. Int J Radiat Biol 1992; 61: 611–24.
37. Hall EJ, Gross W, Dvorak RF, Kellerer AM, Rossi HH. Survival curves and age response functions for Chinese hamster cells exposed to X-rays or high LET alpha particles. Radiat Res 1972; 52: 88–98.
38. Bird RP, Burki HJ. Survival of synchronised Chinese hamster cells exposed to radiation of different linear-energy transfer. Int J Radiat Biol 1975; 27: 105–20.
39. Kraft G. Radiobiological effects of very heavy ions: Inactivation, induction of chromosome aberrations and strand breaks. Nuclear Science Applications 1987; 3: 1–28.
40. Fowler JF. The linear quadratic formula and progress in fractionated radiotherapy. Br J Radiol 1989; 62: 679–94.
41. Thames HD, Withers HR, Peters LJ, Fletcher GH. Changes in early and late radiation responses with altered dose fractionation: implication for dose survival relationship. Int J Radiat Oncol Biol Phys 1982; 8: 219–26.
42. Withers HR. Biological basis for altered fractionation scheme. Cancer 1985; 55: 2086–95.
43. Brahme A. Dosimetric precision requirements in radiation therapy. Acta Radiol Oncol 1984; 23: 379–91.
44. Brahme A. Accuracy requirements and quality assurance of external beam therapy with photons and electrons. Acta Oncol 1988; (Suppl 1): 56–7.
45. Kellerer AM. Fundamentals of microdosimetry. In: Kase, Bjärngard, Attix, eds. The dosimetry of ionizing radiation. Academic Press, 1985; 1: 77–162.
46. Brahme A, Ågren AK. Optimal dose distribution for eradication of heterogeneous tumors. Acta Oncol 1987; 26: 377–85.
47. Bentzen SM, Juul Christensen J, Overgaard J, Overgaard M. Some methodological problems in estimating radiobiological parameters from clinical data. Acta Oncol 1987; 27: 105–16.
48. Turesson I, Thames HD. Repair capacity and kinetics of human skin during fractionated radiotherapy: erythema, desquamation and teleangiectasia after 3 and 5 year follow-up. Radiother Oncol 1989; 15: 169–88.
49. Pihet P, Menzel HG, Schmidt R, Beauduin M, Wambersie A. Biological weighting function for RBE. Specification of neutron therapy beams. Intercomparison of 9 European centres. Radiat Prot Dos 1990; 31: 437–42.
50. Nilsson B. Electron contamination from different materials in high energy photon beams. Phys Med Biol 1985; 30: 139–51.
51. Brahme A, Näfstadius P. Computed dosimetry of scanned electron and photon beams for radiation therapy. Med Phys 1984; 11: 381.
52. Näfstadius P, Brahme A, Nordell B. Computer assisted dosimetry of scanned electron and photon beams for radiation therapy. Radiother Oncol 1984; 2: 261–9.
53. Nilsson B, Brahme A. Contamination of high-energy photon beams by scattered photons. Strahlentherapie 1981; 157: 181–6.
54. Ahnesjö A, Andreo P. Determination of effective bremsstrahlung spectra and electron contamination for photon dose calculations. Phys Med Biol 1989; 34: 1451–64.
55. Andreo P, Brahme A. Stopping power data for high energy photon beams. Phys Med Biol 1986; 31: 839–58.
56. ICRU. Specification of high activity gamma-ray sources. International Commission on Radiation Units and Measurements 1970; Report 18 ICRU, Washington DC.
57. Rogers DWO, Ewart GM, Bielajew AF. Calculation of contamination of the ^{60}Co beam from the AECL therapy source. NRCC Report PXNR-2710 1985; Ottawa.
58. Nordell B, Lindblom E, Montelius A. Energy and lineal energy distributions and absorbed dose components in a 50 MV photoneutron beam. In: Proc. of the Fourth Symposium on Neutron Dosimetry. EUR-7448 Luxembourg CEC 1981; 2: 279–92.
59. Gudowska I. Measurments of neutron radiation around medical electron accelerators by means of ^{235}U chamber and indium foil activation. Radiat Prot Dos 1988; 23: 345–8.
60. Manfredotti C, Nastasi U, Ornato E, Zanini A. Evaluation of the undesired neutron dose equivalent to critical organs in patients treated by linear accelerator gamma ray therapy. Radiat Prot Dos 1992; 44: 457–62.
61. Brahme A, Hultén G, Svensson H. Electron depth absorbed dose distribution for a 10 MeV clinical microtron. Phys Med Biol 1975; 20: 39–46.
62. Andreo P, Brahme A, Nahum A, Mattsson O. Influence of energy and angular spread on stopping-power ratios for electron beams. Phys Med Biol 1989; 34: 751–68.
63. Lax I, Brahme A. Collimation of high energy electron beams. Acta Radiol Oncol 1980; 19: 199–207.
64. Werner BL. Dose perturbations at interfaces in photon beams: Annihilation radiation. Med Phys 1991; 18: 713–8.
65. Lax I. Inhomogeneity corrections in electron-beam dose planning. Limitations with the semi-infinite slab approximation. Phys Med Biol 1986; 31: 879–92.
66. Shortt KR, Ross CK, Bielajew AF, Rogers DWO. Electron beam dose distributions near standard inhomogeneities. Phys Med Biol 1986; 31: 235–49.
67. Nilsson B, Montelius A. Fluence perturbation in photon beams under non equilibrium conditions. Med Phys 1986; 13: 191–5.
68. Kuchnir FT, Reft CS. Experimental determination of fluence perturbation factors for five parallel-plate ionization chambers. Med Phys 1993; 20: 331–5.
69. Montelius A. Neutron dosimetry with detectors of finite size. I: theory. Acta Radiol Oncol 1986; 25: 295–301.
70. Nilsson B, Brahme A. Relation between kerma and absorbed dose in photon beams. Acta Radiol Oncol 1983; 22: 77–85.
71. Magee JL, Chatterjee A. Theoretical aspects of radiation chemistry. In: Farnhataziz and Rodgers MAJ, eds. Radiation chemistry. Principles and applications 1987; 137–171, VCH Verlagsgesellschaft mbH.
72. Paretzke HG. Radiation track structure theory. In: Freeman GR, ed. Kinetics of non-homogeneous processes. John Wiley & Sons 1987: 89–170.
73. Kliauga P, Colvett RD, Goodman LJ, Lam YMO Microdosimetry of 400 MeV/AMU ^{12}C and 450 MeV/AMU ^{40}Ar beams. In: Proc. of the 6th symposium on microdosimetry 1978: 2: 1173–83 Harwood Academic.
74. Söderström S, Gustafsson A, Brahme A. The clinical value of different treatment objectives and degrees of freedom in radiation therapy optimization. Radiother Oncol 1993; 29: 148–63.
75. Tilikidis A, Lind B, Näfstadius P, Brahme A. A microdosimetric investigation on the biological effectiveness of 50 MV scanned bremsstrahlung beams. Int J Radiat Biol 1993, Submitted.